Geochemical characterization of Middle Eocene sediments in Helwan area, Greater Cairo, Egypt

Mohamed M. El Kammar

Geology Department, Faculty of Science, Cairo University, Cairo, Egypt.
Corresponding author : mmelkammar@hotmail.com

Abstract: The Middle Eocene sediments of Qurn and Wadi Garawi formations exposed in the area east of Helwan have been categorized on geochemical basis. Major oxides and trace elements, including the REE, were determined by ICP-MS. This work focuses on the role of the clastic admixture and diagenetic processes on the geochemistry of the marine carbonates. The normalization of the clay-rich limestone to the almost pure limestone points to the significant role of clay admixture as prominent accumulator of trace elements, especially Cu, Pb, Ni, U, Th and REE. The analyzed sediments were generally depleted in Ce, suggesting an influential role of marine conditions, especially when clayey and ferruginous materials are not abundant. The marine versus terrestrial character was best documented by the Y/Ho ratio in the studied sediments. Heavy metals such as Cr, V and As were scavenged by the ferruginous material. The recrystallization of carbonate leads to purification of carbonate sediments, hence, the depletion in content of most major and trace elements. The REE pattern of the recrystallized carbonate displayed clear tetrad effect.
[Mohamed M. El Kammar. **Geochemical characterization of Middle Eocene sediments in Helwan area, Greater Cairo, Egypt.** *Life Sci J* 2013;10(11s):170-178]. (ISSN: 1097-8135). http://www.lifesciencesite.com. 29

Keywords: REE; geochemistry; Maadi Group; limestone; Eocene; Egypt

1. Introduction

The landscape in the Greater Cairo region is intensely imparted by the prominent Eocene limestones hinterlands. The studied limestones, and their stratigraphic equivalent, have traditionally been used for building the pyramids, temples, castles, towers, mosques, monasteries and palaces since the Pharos time to the medieval ages. Sphinx, as well as other status, had also been sculptured in similar limestones. In spite of the cultural worth and the tremendous number of publications on these limestones, the studies on their geochemistry remain insufficient. Moreover, and as far as the author is aware, there is no published data on the geochemistry of the rare earth elements (REE) and isovalent pairs of these sediments. The modern advances on geochemistry implement the REE geochemistry in interpreting the variation in the redox potential of seawater along geologic history (Shields and Stille 2001; Shields and Webb 2004; Ling et al. 2013), characterization of limestone aquifers (Yan et al. 2012; Zhou et al. 2012), dolomitization mechanisms (Zhao and Jones 2012; Haeri-Ardakani et al. 2013), tracing primary and post-depositional geochemical signatures in sedimentary carbonates (Zhao and Zheng 2013) and fractionation during weathering (Zhaoliang et al. 2006). Therefore, the present work provides original complete geochemical data, including the REE and several isovalents, in attempt to interpret the depositional environments and the role of the post depositional activities of the studied limestones.

Geologic Setting

The area under investigation is made up of elevated Eocene limestone plateau. The Upper Eocene sediments are exposed throughout the study area, which lies between latitudes 29° 45' to 29° 50' and longitudes 31° 19' to 31° 25' Fig.1a. The Middle Eocene sedimentary sequence was originally described under the term Unter Mokattamstufe (Zittel 1883). Gabal Mokatam, to the east of Cairo, is accepted by most authors as type locality. The upper limit of the Mokattam Group is clearly marked by changes in facies from white to yellowish compact carbonates to yellow to brown moderately compact marls and sandy limestone of Maadi Group.

The Maadi Group forms a distinct unit which contrasts to the underlying white massive limestone of Mokattam Group Fig.1b.

The sediments of the Maadi Group consist mostly of shales, sandstones intercalated with limestones. The shales are grayish-green highly calcareous and partly sandy. This group is divided in Helwan area into Qurn, Wadi Garawi and Hof formations in ascending order (Farag and Ismael 1959). However, recent studies have shown that the lower two units are well developed in Helwan area and can be assigned as Middle Eocene (Strougo and Boukhary 1987). At El-Qurn height, Qurn Formation is made up of 70 m. thick of white chalky limestone with compact dolomitic limestone bands and yellow marl to marly limestone alternating with shales and sandy marls. The Qurn Formation is overlained conformably by Wadi Garawi Formation with thickness about 25 m. It is characterized by the presence of argillaceous limestones alternating with beds of marls and siltstones.

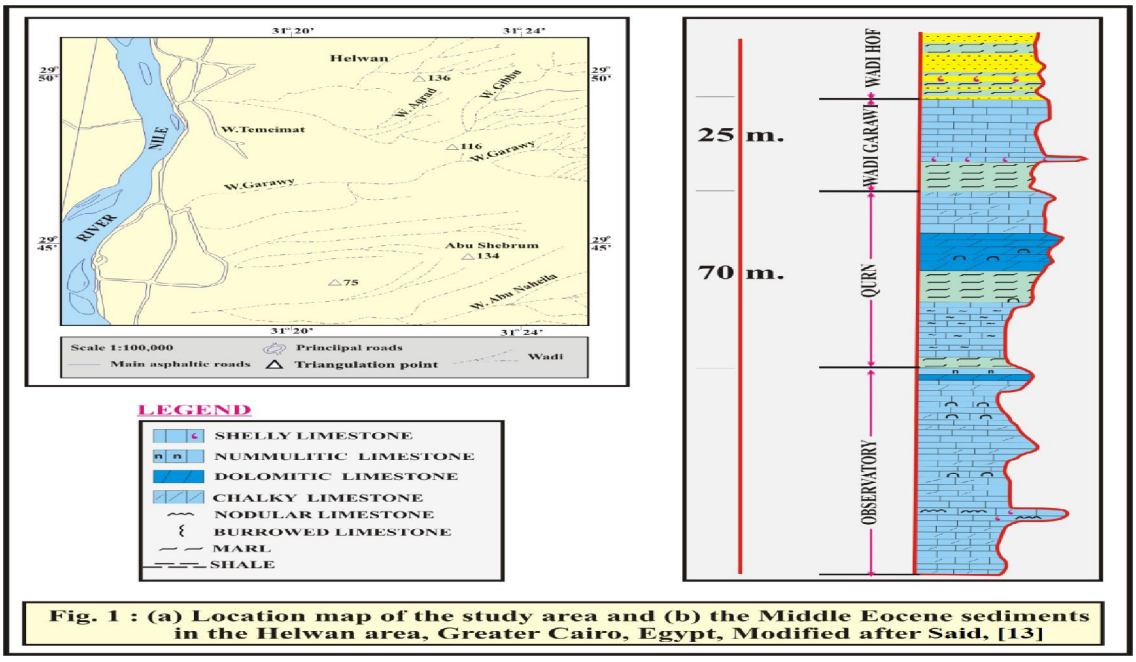

Fig. 1 : (a) Location map of the study area and (b) the Middle Eocene sediments in the Helwan area, Greater Cairo, Egypt, Modified after Said, [13]

The sediments of the Maadi Group consist mostly of shales, sandstones intercalated with limestones. The shales are grayish-green highly calcareous and partly sandy. This group is divided in Helwan area into Qurn, Wadi Garawi and Hof formations in ascending order (Farag and Ismael 1959). However, recent studies have shown that the lower two units are well developed in Helwan area and can be assigned as Middle Eocene (Strougo and Boukhary 1987). At El-Qurn height, Qurn Formation is made up of 70 m. thick of white chalky limestone with compact dolomitic limestone bands and yellow marl to marly limestone alternating with shales and sandy marls. The Qurn Formation is overlained conformably by Wadi Garawi Formation with thickness about 25 m. It is characterized by the presence of argillaceous limestones alternating with beds of marls and siltstones.

The present work aims at better understanding of the role of the clastic admixture and diagenetic processes on the trace elements geochemistry of marine carbonates. Especial emphases are given to the rare earth elements geochemistry.

2.Materials and Methods:

2.1.Materials:

2.1.1.Samples:

Twenty-four samples were collected from surface exposures from the study area to represent the different carbonate facies, as well as, the argillaceous and sandstone intercalations.

2.2.Methods:

The mineral and chemical compositions have been analyzed by X-ray diffraction (XRD) and inductively coupled plasma mass spectrometry (ICP-MS).

2.2.1. Mineral identification:

A Philips Norelco diffract meter with Ni filter and Cu-Kα radiation at 30 kV and 20 mA was used for. The working conditions were kept the same to maintain equal base for comparison of peak intensities as relative measure of mineral abundance.

2.2.2. Examining the subordinate constituents.

The XRD analysis wan done on bulk samples and then repeated once again after removal of calcite by 5% HCl was used

2.2.3. Quantitative determination of trace elements in various materials:

ICP-MS was used for with high precision. About fifty trace elements, including the 14 rare earth elements (REE) were analyzed. The analytical procedure depends on the decomposition of exact weight of 0.2 g powdered sample in 50 ml Teflon beaker. Decomposition was done by 4 ml HNO_3, 3 ml $HClO_4$ and 5 ml HF, and evaporated to dryness under 200°C. The residue was dissolved with 5 ml (1:1) HNO_3 by heating and 5 ml of 4 ppm indium solution was added as an internal standard. The sample solutions were analyzed in the ACME Laboratories in Vancouver, Canada. The obtained data are summarized in Table 1-3.

3. Results and Discussions

This work is based on major oxides and trace elements data as well as the REE of 24 limestone samples representing low-Mg limestones, recrystallized sparite pockets, marl interbeds and sandstone intercalations.

3.1. Mineralogical observations

Calcite is the main carbonate mineral detected in the analyzed 24 samples by the XRD. The argillaceous limestone and sandstone interbeds produce strong reflections related to quartz and clay minerals. Weak reflections that can be interpreted to halite have been recorded in few samples. This halite occurs as surfacial encrustation formed due to evaporation of the capillary water under the prevailing arid climate. Generally speaking, except the interbeds, the studied limestones are exclusively composed of calcitic material.

The diffractograms of the same samples, afterbeing washed with 5% HCl to remove the major calcitic quotient, produce main reflections of quartz, feldspars and clay admixture. Dolomite is detected as minor constituent in only two samples at the lower part of the sedimentary section. Based on the geochemical data of the major elements, the highest MgO content is 0.87% which corresponds to <4% dolomite.

3.2 Marine versus terrestrial

The studied sedimentary exposure represents general period of transgression interrupted by short intervals of regression especially at the lower part (Said 1990). During the short intervals of regression, limestone attains a marly or sandy nature. The trace elements in general and the REE in particular, express such variations in facies and depositional environments. In fact, it is not viable to characterize the trace elements signature of sole marine carbonate since it is not encountered in its pure state. However, the relative contribution of the terrestrial to the marine environments can qualitatively be estimated by normalizing data of the sandy or argillaceous limestone to average limestone relatively poor in silica, alumina and Fe_2O_3.

The normalization of the different limestone facies to the alumina-poor (<1%) limestone indicates that the sandy nature is responsible for the concentration of Zr and Zn, while the argillaceous nature collects some heavy metals as Cu, Pb and Ni, besides Rb which is traditional substitute for K Fig.2. Vanadium is exclusively accumulated by the ferruginous materials. This agrees with the conclusion of Peacock and Sherman (2004) concerning the adsorption via surface complexation of vanadium on goethite under different pH values. They suggested the following empirical equations to explain such adsorption;

$$2FeOH_2^{+}+VO_2^{+}=Fe_2O_2V(OH)_2^{+}+2H^{+}$$
$$2FeOH+HVO_4^{2-}=Fe_2O_2VO(OH)^{0}+2OH^{-}$$

Table 1. Average chemical analysis data (wt. %) of the major oxides

Rock Type / No of samples	Recryst.(1) L.S.	Limestone (<1% Al_2O_3)	Limestone (>1% Al_2O_3)	Arg. (2) L.S.	Ferr. (3) L.S.	Calc. (4) S.S.
	n = 2	n = 8	n = 10	n = 2	n = 1	n = 1
SiO_2	1.4	4.37	7.63	22.97	16.4	79.1
TiO_2	0.02	0.03	0.08	0.57	0.18	0.62
Al_2O_3	0.14	0.66	1.46	10.68	3.23	3.89
Fe_2O_3	0.27	0.72	1.23	2.64	7.73	2.72
MgO	0.36	0.34	0.4	0.68	0.87	0.35
CaO	53.27	50.99	47.98	30.86	37.44	6.05
Na_2O	0.02	0.03	0.04	0.08	0.03	0.04
K_2O	0.04	0.09	0.17	0.85	0.08	0.47
P_2O_5	0.01	0.02	0.02	0.15	0.19	0.16
H_2O^-	0.14	0.2	0.2	0.62	0.56	0.27
L.500	0.48	0.32	0.4	1.51	1.28	0.83
LOI	42.94	41.85	40.07	27.7	31.9	5.9

(1) Recryst. L.S.= Recrystallized Limestone (2) L.S.= Argillaceous Limestone
(3) Ferr. L.S.= Ferruginous Limestone (4) Calc. S.S.= Calcareous Sandstone

Table 2: Average ICP-MS analysis data (ppm) of trace elements

Rock Type / No. of samples	Recryst.(1) L.S.	Limestone (<1% Al_2O_3)	Limestone (>1% Al_2O_3)	Arg. (2) L.S.	Ferr. (3) L.S.	Calc. (4) S.S.
	n = 2	n = 8	n = 10	n = 2	n = 1	n = 1
Mn	64	217	273.1	277	320	149
Cu	3.5	2.8	3.7	9	5	6
Pb	7	5.6	7.2	18	7	5
Zn	7.5	6.9	13.2	21	26	54
Ni	4.5	6	11.4	29	22	16
As	5	8.3	7.4	14	15	5
V	10	10.5	17.3	85	156	42
Cr	8.0	7.9	12.9	56	47	33
Rb	1.1	2.8	5.8	32.4	3.3	16.2
Sr	798	720	840	836	980	231
Ba	9	17	13	42	30	67
Zr	2.0	3.1	6.9	53	20	109
Th	2.05	0.85	1.21	5.5	3.3	6.2
U	1.65	2.54	2.25	2.2	1.2	4.5

(1) Recryst. L.S.= Recrystallized Limestone (2) L.S.= Argillaceous Limestone
(3) Ferr. L.S.= Ferruginous Limestone (4) Calc. S.S.= Calcareous Sandstone

Table 3. Average ICP-MS data (ppm) of Y and REE

Rock Type / No. of samples	Recryst.(1) L.S.	Limestone (<1% Al_2O_3)	Limestone (>1% Al_2O_3)	Arg. (2) L.S.	Ferr. (3) L.S.	Calc. (4) S.S.
	n = 2	n = 8	n = 10	n = 2	n = 1	n = 1
Y	1.2	8.4	11.6	27.7	24.1	33.0
La	0.9	6.1	7.6	25.9	14.2	18.3
Ce	1.1	6.4	13.5	51.7	26.2	36.9
Pr	0.31	1.4	2.3	7.7	4.4	6.1
Nd	1.34	6.14	9.5	29.9	18.1	26.0
Sm	0.19	1.33	2.06	6.37	4.32	6.25
Eu	0.09	0.40	0.59	1.59	1.24	1.46
Gd	0.2	1.4	2.1	6.0	4.5	5.8
Tb	0.04	0.26	0.39	1.13	0.90	1.13
Dy	0.16	1.33	2.11	5.86	5.06	6.65
Ho	0.04	0.28	0.42	1.15	1.02	1.41
Er	0.12	0.77	1.18	3.25	2.92	4.34
Tm	0.02	0.09	0.15	0.44	0.42	0.69
Yb	0.08	0.55	0.93	2.84	2.69	4.76
Lu	0.01	0.06	0.11	0.33	0.32	0.66
REEs	4.6	26.5	42.92	144.13	86.35	120.35

(1) Recryst. L.S.= Recrystallized Limestone (3) Ferr. L.S.= Ferruginous Limestone
(4) Calc. S.S.= Calcareous Sandstone
(2) L.S.= Argillaceous Limestone

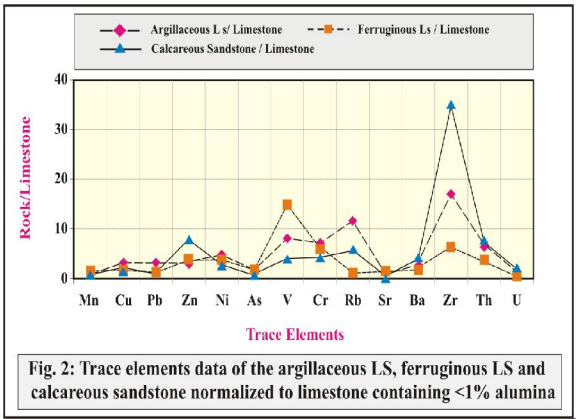

Fig. 2: Trace elements data of the argillaceous LS, ferruginous LS and calcareous sandstone normalized to limestone containing <1% alumina

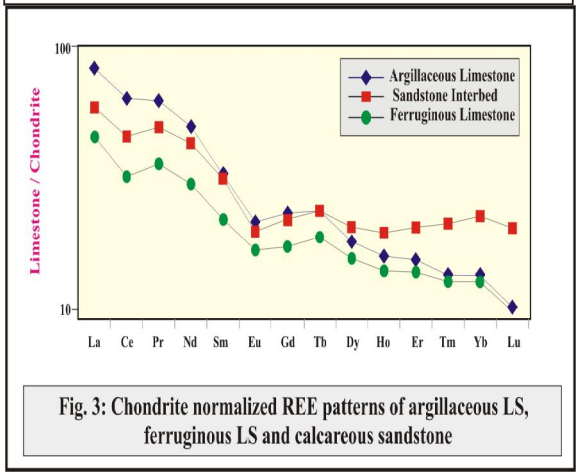

Fig. 3: Chondrite normalized REE patterns of argillaceous LS, ferruginous LS and calcareous sandstone

3.3 REE distribution

According to Zhao and Jones (2012), despite their complex diagenetic history, the limestones and dolostones, of their study area, inherited seawater-like REE+Y patterns. The normalization of the REE content of the different facies to chondrite Fig.3, suggests the following important observations:

1. The calcareous sandstone pattern displays marked enrichment in the heaviest REE. This can be attributed to contribution of detrital zircon.
2. The argillaceous limestone displays distinct increase in the light REE possibly due to presence of LREE-bearing minerals occurring in the mud size.
3. The ferruginous material seems to be insignificant accumulator of the REE.
4. In response to the prevailing marine environment, all facies display clear negative Ce anomaly.

In spite of the fact that the influence of zircon is well expressed by the relative enrichment of the heaviest REE in the calcareous sandstone intercalation, it seems that the total REE budget is principally controlled by uptake from the Ce-deficit seawater. The role of the Ce deficiency is well illustrated by the strong correlation between the Ce anomaly (mostly on the negative side) and ΣREE Fig.4.

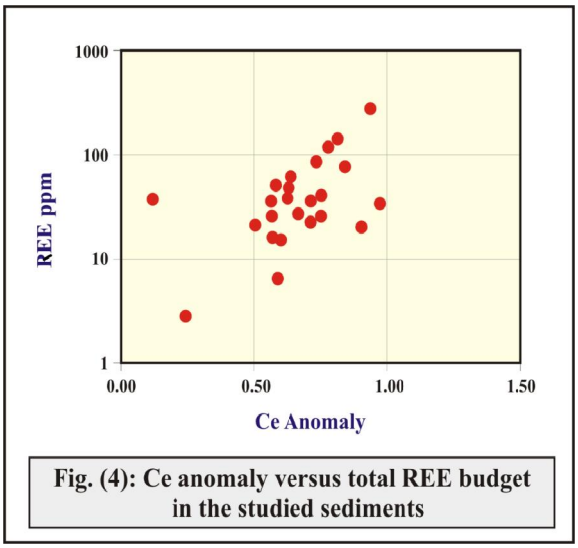

Fig. (4): Ce anomaly versus total REE budget in the studied sediments

The REE budget increases with decreasing the Ce deficiency (i.e., relative increase in Ce content) as a result of increasing non-carbonate admixture. The latter is less-deficit in cerium than marine carbonates. This agrees with Ling et al. (2013) and Tang et al. (2012) who believe that Ce anomalies can be used to trace oxygenation changes in seawater. They quoted that the magnitude of the negative Ce anomaly in seawater is related to dissolved oxygen concentration, and in modern fully oxygenated deep oceans, the dissolved REE load exhibits the most negative Ce anomalies.

3.4. Uranium-Thorium relation

Except the ferruginous limestone, all the analyzed sediments have non-chondritic Th/U ratio, toward higher uranium, especially in the limestone containing less than 1% Al_2O_3 Fig.5. The high permeability and porosity of the carbonate sediments during early diagnosis (Tanaka and Kawabe 2006) are necessary for seawater uranium incorporation into marine limestone. No doubt that the terrestrial admixture can incorporate much higher quotient of the Th together with other elements having short residence time in seawater such as Zr and Cr.

3.5. Role of clay admixture

The studied limestone succession contains argillaceous limestone beds especially at its lower part of the sequence. The alumina content varies between 0.47 and 10.88%, but decreases to 0.11% in the recystallized sparite pockets. The alumina content, even at its lower concentration magnitude, seems to be influential as trace elements accumulator.

The SiO_2/Al_2O_3 ratio varies between 2.5 and 22, averaging 6.6, suggesting that considerable quotient of silica exists in the free state which is determined petrographically to be detrital quarts of

different grain sizes. However, alumina shows strong positive correlation with K_2O (r^2 = 0.9) suggesting preponderance of illitic clays.

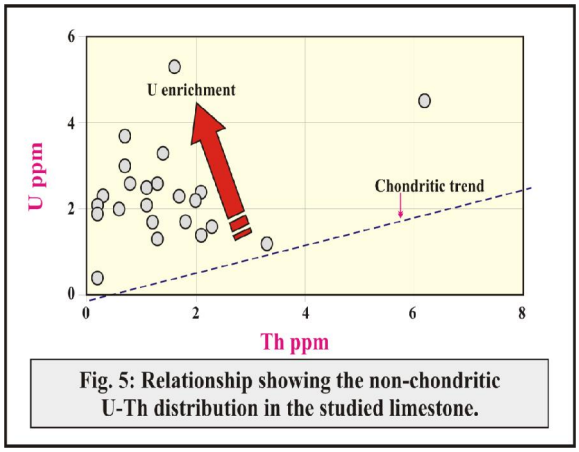

Fig. 5: Relationship showing the non-chondritic U-Th distribution in the studied limestone.

The correlation matrix of the analyzed major and trace elements shows intimate coherence among some heavy metals, namely; Cu, Pb and Ni with alumina, while others (e.g., Cr, V and As) are better correlated to Fe_2O_3. This sort of portioning among heavy metals indicates different speciation and/or sources. At first glance, it appears that the alumina rich samples contain higher REE budget Table 3. In order to quantify the role of alumina, as an immediate expression of clay mineral fraction, on the REE distribution and abundance, the samples have been classified into two categories, namely alumina-poor (< 1% Al_2O_3) and alumina-rich (> 1% Al_2O_3). Both varieties have been normalized to the geometric mean of the Tahara Limestone in central Japan as quoted by Tanaka et al. (2003). The normalized REE patterns Fig.6, indicate the following assumptions:

1. The REE content of the alumina-rich limestone is 2 to 3 fold that of the alumina-poor variety, suggesting that alumina is certainly a powerful accumulator of REE.
2. The alumina-rich limestone is diagnostically characterized by strong positive anomaly of cerium (ΔCe=1.64). This can be attributed to the influence of detrital Ce-bearing minerals such as monazite.

Apart from the higher REE budget and the +ΔCe anomaly of the alumina-rich limestone, the normalized patterns of the two varieties are closely similar. Both patterns display marked Gd break with relative enrichment of the middle REE (bell-shape). Kidder and Eddydilek (1994) suggest that the initial MREE enrichment mechanism may be analogous to that in which some modern algae preferentially extract MREE from water of marine composition. The contribution by Frimmel (2009) confirms that the REE+Y patterns of limestone cannot be ascribed solely to shale contamination but are interpreted as resulting from the incorporation of near-shore colloids, possibly related to Fe-oxy-hydroxide scavenging.

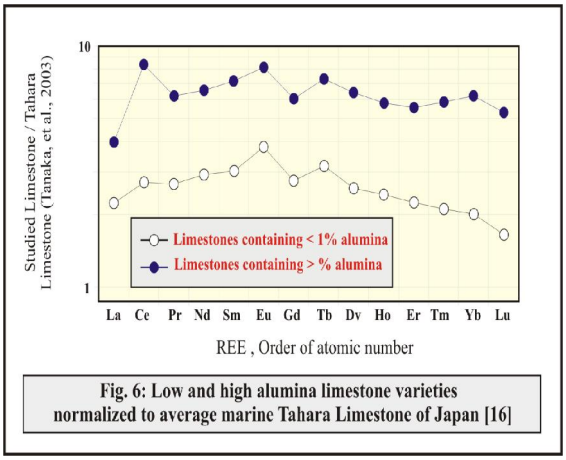

Fig. 6: Low and high alumina limestone varieties normalized to average marine Tahara Limestone of Japan [16]

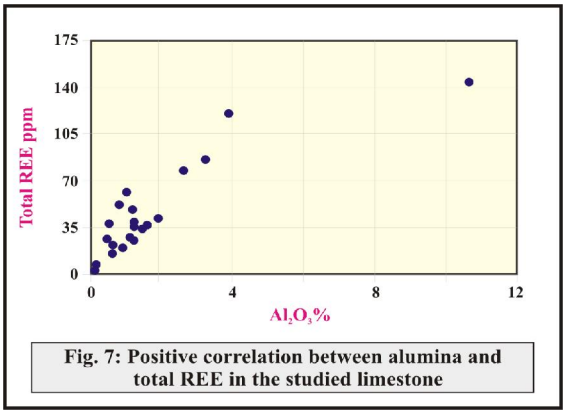

Fig. 7: Positive correlation between alumina and total REE in the studied limestone

The positive correlation between alumina and total REE content Fig.7, suggests that every 1% of clays in the studied sediments accumulate about 30 ppm of REE. Similar observation was noted by Thomas (1994) who stated that in the more impure limestones, the dominant control on REE content was the clay mineral content in siliciclastic impurities derived from terrestrial sources. The dependence of the total REE concentration in limestones on shale contamination has recently been ascertained by Frimmel (2009). However, the role of clays as REE accumulator is not that simple and it seems to be governed by wide range of physico-chemical parameters. According to Junya et al. (2002), the spatial distribution of REE in marine sediments bears much information about the supply of sediments in different sea areas, the distance between sedimentary region and seashore, seawater depth, redox conditions, the influence of climate on the ocean, submarine volcanic activity and so on. Temporal

variations of REE in marine sediments can shed light on the history of oceanic changes in the long geological past so as to provide the grounds for the study of geotectonic activity, sea-level change and paleo-ocean environmental and paleoclimatic changes.

3.6. Yttrium/Holmium ratio

Y and Ho are isovalent, having the same charge and radius. This ratio is about 28 in the upper continental crust as cited by Taylor and McLennan (1985) and about 26 in Australian sediments as quoted by Kamber et al. (2005). The Y/Ho ratio performs authentic fractionation in the marine environments, mainly because Ho is preferentially removed from seawater twice as fast as Y because of differences in the surface complexation behavior (Nozaki et al. 1997). Therefore, several authors have used the Y/Ho ratio to observe the differentiation between marine and non-marine deposits (Bau 1996; Nothdurft et al. 2004; Frimmel 2009). Moreover, Lawrence et al. (2006) recorded Y/Ho ratio between 60 and 90 in open seawater and added that it is strongly dependent on salinity. In the present work, the average of Y/Ho ratio (n=24) is 26 which is the same average ratio determined for the Australian sediments (Kamber et al. 2005). In agreement with Frimmel (2009), there is systematic fractionation of Y/Ho towards lower values (24) in the alumina-rich limestone and increases up to 36 in the alumina-poor limestone Fig.8.

3.7. Role of ferruginous material

The accumulation of heavy metals (Peacock and Sherman 2004) or REE (Frimmel 2009) on ferruginous material via scavenging is a known feature. In the present work, the efficiency of alumina (clay fraction) as good accumulator of some heavy metals and the REE has been examined. It seems that clays are not the sole accumulator of trace metals but ferruginous materials can be nominated as partner. The plot of the correlation coefficients among heavy metals, including iron, shows the clear fractionation of these metals Fig.9. Some of the heavy metals show clear dependence on iron content, such as V and Cr, while others, such as Pb and Zn, seem not to be dependent on scavenging by iron.

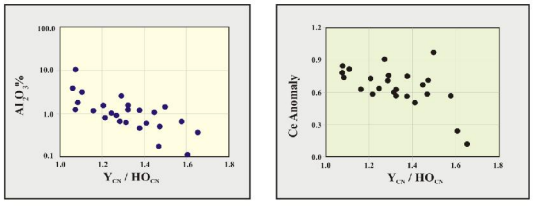

Fig. 8: Chondrite normalized Y/Ho ratio versus Alumina and cerium anomaly.

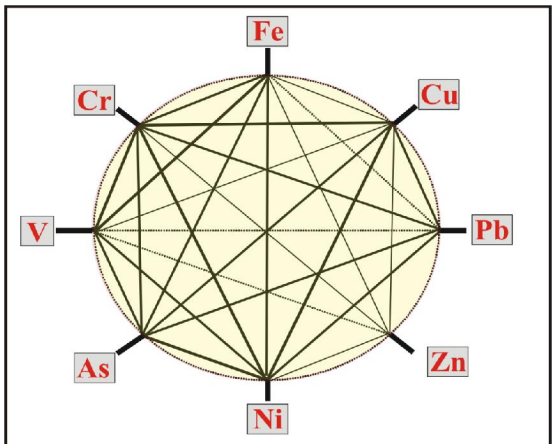

Fig. 9: Correlation coefficients among heavy metals in the studied sediments (Intensity of lines correspond to strength of correlation coefficient with highest r2=>0.8 and least 0.3).

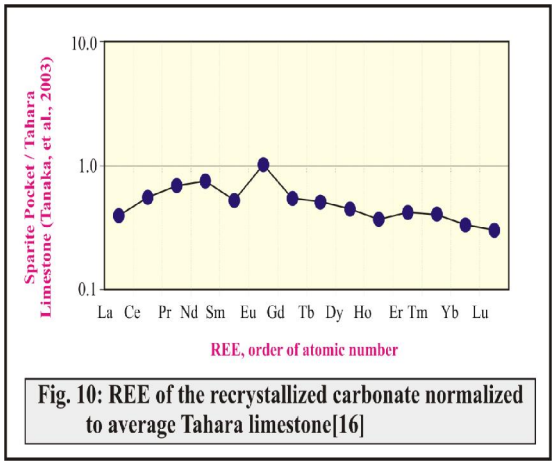

Fig. 10: REE of the recrystallized carbonate normalized to average Tahara limestone[16]

3.8. Role of carbonate recrystallization

At the uppermost part of the studied section, pocket and veins filled with aggrading recrystallized sparite are considered in the present work in order to evaluate the chemical changes accompanying such process. On geochemical basis, it is evident that the recrystallization is a purification process where the CaO content reaches 53.7% which corresponds to about 96% $CaCO_3$.

Indeed, these recrystallized carbonates contain the least concentrations of most insoluble oxides such as; SiO_2, TiO_2, Al_2O_3, Fe_2O_3 and K_2O. Moreover, the purification process extends to cover almost all the analyzed trace elements, including the REE and Y. However, it seems that the dissolution and re-precipitation of calcite cause selective removal and uptake of the REE possibly under the control tetrad effect phenomena Fig.10. Fairchild and Treble (2009) reported recently that elements, other than the divalent ones such as Mg, Sr and Ba, may be

incorporated in $CaCO_3$ by different mechanisms. For example, the element may be transported by water and incorporated in the speleothem associated with either fine detrital particles, or as sub-micron-sized colloids. Lower concentrations of such elements (e.g., REE) would be expected in water and in associated speleothems during periods of lower infiltration. However, the REE content is, generally, lower than that of the Tahara Limestone (Tanaka et al. 2003), except Eu which produces marked positive anomaly. The obtained pattern displays mild M-type tetrad effect, especially the first tetrad (t_1) of La-Nd.

Conclusions

At El-Qurn height, Qurn and Wadi Garawi formations are made up of limestone alternated with marls, marly limestone, argillaceous limestone, sandy marl and shale.

Calcite is the main carbonate mineral detected in most samples by the XRD. The argillaceous limestone and sandstone intercalations produce strong reflections related to quartz and clay minerals. Weak reflections can be interpreted to halite. Dolomite was detected as minor constituent in only two samples at the lower part of Qurn Formation.

The studied sedimentary exposure represents general period of transgression interrupted by short intervals of regression especially at the lower part. During these short intervals, limestone attains a marly or sandy nature. The trace elements in general and the REE in particular, express such variation in facies and depositional environments. The increase of the terrestrial admixture improves the REE budget and decreases the Ce deficiency. However, the relative contribution of the terrestrial to the marine environments can qualitatively be estimated by normalizing data of the sandy or argillaceous limestone to average limestone. This suggests that the sandy nature is responsible for the concentration of Zr and Zn, while the argillaceous matter enhances some the heavy metals, as Cu, Pb and Ni, besides Rb. Vanadium is mostly scavenged by the ferruginous materials.

No doubt that the terrestrial admixture concentrates much higher proportion of Th and the other elements that have short residence time in seawater such as Zr and Cr. The alumina content, even at its lower concentration magnitude, seems to be influential accumulator of trace elements in general and REE in particular. The alumina-rich limestone accrues 2 to 3 fold of REE relative to the alumina-poor variety, suggesting that alumina is certainly a powerful accumulator of REE. The positive correlation between alumina and total REE content suggests that every 1% of clay in the studied sediments accumulates about 30 ppm of REE. However, the role of clays as REE accumulator is not that simple and it seems to be governed by wide range of physico-chemical parameters. There is a systematic fractionation of Y/Ho towards lower values in the alumina-rich limestone.

On geochemical basis, it is evident that the recrystallization is a purification process where CaO content reaches 53.7% which corresponds to about 96% $CaCO_3$. The REE content is, generally, lower than published data on pure limestone, except Eu which produces marked positive anomaly. The obtained pattern displays mild M-type tetrad effect, especially the first tetrad (t_1) of La-Nd.

References

1-Bau, M. 1996. Controls on fractionation of isovalent trace elements in magmatic and aqueous systems: evidence from Y/Ho, Zr/Hf, and lanthanide tetrad effect. *Contrib Mineral Petr*. 123, 323–333.

2-Fairchild, IJ. and Treble, PC. 2009. Trace elements in speleothems as recorders of environmental change. *Quaternary Sci Rev*. 11, 007.

3-Farag, IAM. and Ismail, MM. 1959. A contribution to the stratigraphy of the wadi Hof area northeast of Helwan. *Bull Fac Sci Cairo Univ*. 34, 147-168.

4-Frimmel, H. 2009. Trace element distribution in Neoproterozoic carbonates as palaeoenvironmental indicator. *Chem Geol*. 258 (3–4), 30, 338-353.

5-Haeri-Ardakani, O., Al-Aasm, I. and Coniglio, M. 2013. Petrologic and geochemical attributes of fracture-related dolomitization in Ordovician carbonates and their spatial distribution in southwestern Ontario Canada. *Mar Petrol Geol*. doi:10.1016/j.marpetgeo.2012.12.006.

6-Junya, N., Congqiang, L., Dequan, Z. and Zhuming, W. 2002. REE geochemical study of the Permian-Triassic marine sedimentary environment in Guizhou Province. *Chinese J Geochem*. 21 (4), 348-361.

7-Kamber BS, Greig A, Collerson KD. (2005). A new estimate for the composition of weathered young upper continental crust from alluvial sediments, Queensland, Australia. *Geochim Cosmochim Ac.* 69, 1041–1058.

8-Kidder, D. and Eddydilek, C. 1994. Rare-earth element variation in phosphate nodules from midcontinent Pennsylvanian cyclothems. *J Sediment Res*. 64 (3), 584-592.

9-Lawrence, M., Greig, A., Collerson, KD. and Kamber, BS. 2006. Rare earth element and yttrium variability in South East Queensland waterways. *Aquat Geochem*. 12, 39–72.

10-Ling, HF., Chen, XLiD., Wang, D., Shields, G., Zhoub, A. and Zhu, M. 2013. Cerium anomaly variations in Ediacaran–earliest Cambrian carbonates from the Yangtze Gorges area, South China: Implications for oxygenation of coeval shallow seawater. *Precambrian Res.* 225, 110-127.

11-Nothdurft, LD., Webb, GE. and Kamber, BS. 2004. Rare earth element geochemistry of Late Devonian reefal carbonates, Canning Basin, Western Australia: confirmation of a seawater REE proxy in ancient limestones. *Geochim Cosmochim Ac.* 68, 263–283.

12-Nozaki, Y., Zhang, S. and Amakawa, H. 1997. The fractionation between Y and Ho in the marine environment. *Earth Planet. Sc Lett.* 148, 329-340.

13-Peacock, CL. and Sherman, DM. 2004. Vanadium (V) adsorption onto goethite (α-FeOOH) at pH 1.5 to 12: a surface complexation model based on molecular geometries and EXAFS spectroscopy. *Geochim Cosmochim Ac.* 68 (8), 1723-1733.

14-Said, R. 1990. *The geology of Egypt*. AA Balkema, Rotterdam, Netherlands.

15-Shields, G. and Stille, P. 2001. Diagenetic constraints on the use of cerium anomalies as palaeoseawater redox proxies: an isotopic and REE study of Cambrian phosphorites. *Chem Geol.* 175, 29–48.

16-Shields G, Webb G. (2004). The REE composition of seawater changed over geological time? *Chem Geol.* 204, 103– 107.

17-Strougo, A. and Boukhary, M. 1987. The Middle Eocene – Upper Eocene boundary in Egypt: Present state of the problem. *Rev Micropaleontol.* 1987, 30.

18-Tanaka, K. and Kawabe, I. 2006. REE abundance in ancient seawater inferred from marine limestone and experimental REE partition coefficient between calcite and aqueous solution. *Geochem J.* 40, 425-435.

19-Tanaka, K., Miura, N., Asahara, Y. and Kawabe, I. 2003. Rare earth elements and Sr isotopic study of Southern Chichibu Terrane, Central Japan: Implecation for incorporation process of seawater REE into limestone. *Geochem J.* 37, 163-180.

20-Taylor, SR. and McLennan, SM. 1985. *The Continental Crust: Its Composition and Evolution.* Blackwell Oxford.

21-Thomas, CW. 1994. Sources of rare earth elements in Appin Group limestones, Dalradian, north-east Scotland. *Miner Petrol.* 51, 239.

22-Yan, Z., Liu, G., Sun, R., Tang, Q., Wu, D., Wu, B. et al. 2012. Geochemistry of rare earth elements in groundwater from the Taiyuan Formation limestone aquifer in the Wolonghu Coal Mine, Anhui province, China. *J Geochem Explor*. doi:10.1016/j.gexplo.2012. 11.011

23-Zhao, H. and Jones, B. 2012. Distribution and interpretation of rare earth elements and yttriumin Cenozoic dolostones and limestones on Cayman Brac, British West Indies. *Sediment Geol* (2012). doi:10.1016/j.sedgeo.10.009.

24-Zhao, YY. and Zheng, YF. 2013. Geochemical constraints on the origin of post-depositional fluids in sedimentary carbonates of the Ediacaran system in South China. *Precambrian Res.* 224, 341– 363.

25-Zhaoliang, S., Congqiang, L., Guilin, H., Zhongliang, W., Zhaozhou, Z. and Cheng, Y. 2006. Enrichment and release of rare earth elements during weathering of sedimentary rocks in Wujiang catchments Southwest China. *J Rare Earth.* 24, 491 – 496.

26-Zhou, H., Greig, A., Tang, J., You, CF. and Yuan, D. 2012. Rare earth element patterns in a Chinese stalagmite controlled by sources and scavenging from karst groundwater. *Geochim Cosmochim Ac.* 2012; 83, 1–18.

27-Zittel. 1883. Beitrage zur geologie und palaeontologie der Libyschen wuste und der angrenzenden gebiete von Aegypten. *Palaeontographica.* 1883; 30(3F), 1, 147, 2, 237.

10/2/2013